Elucidation of the reaction mechanism of indirect oxidative carbonylation of methanol to dimethyl carbonate on Pd/NaY catalyst: Direct identification of reaction intermediates

Chunzheng Wang, Bin Liu, Panyue Liu, Ke Huang, Ningkun Xu, Hailing Guo, Peng Bai, Lixia Ling, Xinmei Liu, Svetlana Mintova

Elucidation of the reaction mechanism of indirect oxidative carbonylation of methanol to dimethyl carbonate on Pd/NaY catalyst: Direct identification of reaction intermediates

Chunzheng Wang,[a,*] Bin Liu,[a] Panyue Liu,[b] Ke Huang,[a] Ningkun Xu,[a] Hailing Guo,[a] Peng Bai,[a] Lixia Ling,[b,*] Xinmei Liu,[a] Svetlana Mintova[a,c,*]

[a] *State Key Laboratory of Heavy Oil Processing, College of Chemical Engineering, China University of Petroleum (East China), Qingdao 266580, Shandong, China*

[b] *College of Chemistry and Chemical Engineering, Taiyuan University of Technology, Taiyuan 030024, Shanxi, China*

[c] *Laboratoire Catalyse et Spectrochimie (LCS), Normandie Université, ENSICAEN, UNICAEN, CNRS, 6 boulevard Maréchal Juin, Caen 14050, France*

[*] Corresponding authors. E-mail addresses: czwang@upc.edu.cn (C. Wang), linglixia@tyut.edu.cn (L. Ling), svetlana.mintova@ensicaen.fr (S. Mintova)

Abstract

Gas-phase indirect oxidative carbonylation of methanol to dimethyl carbonate (DMC) has been industrialized, but the reaction mechanism is still ambiguous. In this work, the reaction mechanism of DMC synthesis using a NaY zeolite catalyst doped

with 1.0 wt% Pd was revealed by combining *in situ* diffuse reflectance infrared Fourier transform spectroscopy (DRIFTS) results with density functional theory (DFT) calculations. Two key reaction intermediates CO* (*, a surface site) and $COOCH_3$* were identified through the adsorption of a probe molecule of methyl chloroformate (CH_3OCOCl), and characterized by steady-state, dynamic-pulse and time-resolved transient DRIFTS experiments. The CO* intermediate is predominant on the catalyst surface when the reaction reached steady-state. The DFT results also showed that the inclusion of OCH_3* into CO* had the highest energy barrier of 127.5 kJ mol^{-1}. This verified that the formation of $COOCH_3$* is the rate-determining step for the DMC synthesis. A Langmuir-Hinshelwood mechanism including the fast formation of CO*, and rate-determining insertion of OCH_3* into CO* toward generation of $COOCH_3$* to yield DMC was proposed.

Keywords: DRIFTS; Palladium; NaY; Zeolite; Reaction intermediate; Dimethyl carbonate; Methanol

1. Introduction

C1 chemistry addressing the transformations of one-carbon molecules such as CO, CO_2, CH_3OH and CH_4 [1,2], is becoming very important due to the increasing need to produce valuable liquid fuels and chemicals, from alternative carbon resources such as natural gas, shale gas and CO_2 emissions [3,4]. Dimethyl carbonate (DMC) is

considered as a promising sustainable reagent because of its excellent biodegradability, low toxicity and high versatility [5]. As a platform raw material, the DMC is widely applied as an electrolyte solvent in lithium-ion batteries, potential fuel additive, in polymer synthesis (polycarbonates, polyurethanes and non-isocyanate polyurethanes), and as carbonylation and methylation reagents instead of the toxic phosgene and dimethyl sulfate [6]. The traditional production of DMC involves the utilization of hypertoxic phosgene ($COCl_2$). Thus, several phosgene-free routes have been developed for the synthesis of DMC, including the direct/indirect oxidative carbonylation of methanol (CH_3OH), conversion of CO_2 and CH_3OH, transesterification of cyclic carbonates and CH_3OH, and urea methanolysis [7–9]. Among these processes, the indirect oxidative carbonylation of methanol to DMC has attracted ever-growing interest due to the high atom efficiency, waste avoidance, simple operation and cheap raw materials [10]. The indirect process consists of two main reactions: (1) Pd-catalyzed oxidative carbonylation to DMC: $CO + 2CH_3ONO \rightarrow (CH_3O)_2CO + 2NO$, and (2) non-catalytic methyl nitrite (CH_3ONO) regeneration with recycled NO: $2CH_3OH + 2NO + 1/2O_2 \rightarrow 2CH_3ONO + H_2O$. The overall reaction ($CO + 2CH_3OH + 1/2O_2 \rightarrow (CH_3O)_2CO + H_2O$) is a highly-efficient and environmentally-benign process converting C1 feedstocks (CO and CH_3OH) to C2 chemical.

The gas-phase indirect oxidative carbonylation of methanol to DMC has been industrialized by Ube Industries, Ltd., Japan (15000 tons/year), using a

$PdCl_2$/active-carbon catalyst [11,12]. Although the chlorine-containing catalyst showed excellent initial activity and selectivity, it would be rapidly deactivated because of the loss of chlorine element [13]. In fact, the chloride, such as 100 μL L^{-1} HCl must be added into the feed gas to maintain the stability and activity of the chlorine-containing catalyst, which inevitably leads to the equipment corrosion, difficult regeneration of chlorine, and unqualified purity of DMC product [14]. Therefore, substantial efforts are dedicated to the development of chlorine-free Pd-based catalysts. In the past decade, the effects of catalyst supports (NaY, NaX, NaEMT, γ-Al_2O_3, α-Al_2O_3, SiO_2, MgO and MOF) [15–17], promoters (Cu and K elements) [18,19], Lewis and Brønsted acid sites [20], and various Pd species [21–23] have been intensively investigated to improve the catalytic performance of the chlorine-free catalysts. However, the catalytic reaction mechanism is far from being clear on the chlorine-free Pd-based catalysts.

Yamamoto et al. suggested a possible reaction mechanism on the chlorine-free Pd/NaY catalyst [14,24]. The reaction was initiated by the oxidative addition of CH_3ONO reactant to form NO–Pd–OCH_3 intermediate, followed by the insertion of CO reactant to generate NO–Pd–$COOCH_3$ intermediate. Subsequently, another CH_3ONO coupled with NO–Pd–$COOCH_3$ to yield DMC by the reductive elimination was proposed. According to the kinetic study, it was found that the reaction order was about one with respect to CH_3ONO reactant, but was zero with respect to CO reactant. Based on these results, it was inferred that the rate-determining step was associated

with CH_3ONO. Uchiumi et al. reported that DMC was selectively formed on the oxidized catalyst rather than reduced catalyst, and hence assumed that Pd^{2+} instead of Pd^0 species were the catalytic active sites [11]. The XPS results demonstrated that the used Pd/NaY catalyst contained Pd^{2+} and Pd^0 species [17,18,24]. Tan et al. considered that Pd^{2+} was the catalytic active sites, while Pd^0 was an intermediate to be re-oxidized to Pd^{2+} through oxidative addition of CH_3ONO reactant [21]. The EXAFS results by Yamamoto et al., suggested that the aggregation of Pd^0 species took place during the DMC synthesis, forming stable Pd_{13} clusters on the Pd/NaY catalyst [24]. Similar results were also reported by Dong and Wang et al. [17,18]. Tan et al. concluded based on DFT calculations, that the DMC formation followed an Eley-Rideal (E-R) mechanism rather than Langmuir-Hinshelwood (L-H) mechanism, using an active site model of palladium acetylacetonate [$Pd(acac)_2$] [22]. They revealed that the adsorbed CO could react with gas-phase CH_3ONO reactant to form DMC via E-R mechanism. This was inconsistent with that the adsorption of CH_3ONO reactant was generally considered as the first step for the DMC formation [14,24].

The reaction mechanism of DMC synthesis was discussed in several articles [10,13,22,24]. Still the reaction pathways presented have not been supported experimentally, and the reaction intermediates and rate-determining step of DMC formation are not experimentally revealed yet. It is still under debate whether the DMC synthesis is described by the L-H or the E-R mechanisms.

Monitoring the surface phenomena occurring on the catalysts under different

reaction conditions is essential for clarifying the nature of active sites, reaction pathways, possible reaction intermediates, and establishing the structure-activity/selectivity relationship [25,26]. Such knowledge is beneficial to rational design and fine tuning of new-type catalysts. *In situ* DRIFTS spectroscopy, is a very powerful tool applied to monitor the formation and accumulation of adsorbed reactants, reaction intermediates, and/or side products on the catalyst surface [27,28]. Nevertheless, it is difficult to identify the chemical structure of reaction intermediates only by the DRIFTS spectroscopy [29]. DRIFTS characterization is often combined with other techniques such as DFT, Raman, UV-vis, etc. toward investigation of the reaction mechanism [30–32].

As previously reported, a high-performance Pd/NaY catalyst was developed for the indirect oxidative carbonylation of methanol to DMC [23]. The tableting pressure applied to the Pd/NaY catalyst was found to have a pronounced effect on the Pd active sites. In the current paper, a series of *in situ* DRIFTS experiments involving adsorption/desorption of CO and CH_3ONO reactants, steady-state DMC synthesis, dynamic-pulse reactions of CO and CH_3ONO reactants, and time-resolved transient reactions using a probe molecule (CH_3OCOCl) were conducted to capture the reaction intermediates and elucidate the reaction pathways on the Pd/NaY catalyst. Additionally, DFT calculations and a detailed kinetic study were performed to reveal the reaction mechanism of indirect oxidative carbonylation of methanol to DMC on the Pd/NaY catalyst.

2. Experimental

2.1. Catalyst preparation

The catalyst was prepared as described elsewhere [23]. In a typical process, 1.0 g NaY zeolite (Daqing Chemical Research Center, China) was added into 100 mL deionized water and stirred for 2 h to form a suspension. 16.7 mg palladium chloride ($PdCl_2$, Sinopharm Chemical Reagent Co., Ltd., China) was dissolved in 1.2 mL, 0.94 mol L^{-1} ammonia (NH_3) solution to form a clear palladium ammonia complex ($Pd(NH_3)_4Cl_2$) solution, and then added dropwise into the NaY zeolite suspension. The resulting suspension was stirred at 25 ºC for 12 h, and then heated at 80 ºC to remove the excess ammonia until the pH value of the suspension decreased to 7.0–7.2. After that, the solid precipitate was filtered and washed with deionized water. The obtained material was dried at 80 ºC for 6 h and then calcined in air at 200 ºC for 2 h with a heating rate of 0.5 ºC min^{-1}. Finally, the catalyst was pelleted, crushed and sieved into a size of 60–80 mesh. This catalyst was denoted as Pd/NaY.

The as-prepared Pd/NaY catalyst had a Si/Al molar ratio of 2.8 and a Pd content of 1.0 wt% as determined by inductively coupled plasma-atomic emission spectroscopy (ICP-AES). The chlorine was not detected in the sample by the elemental mapping of energy dispersive X-ray spectrometer (EDS; Fig. S1), suggesting that the as-prepared Pd/NaY catalyst was chlorine-free. The catalytic performances of the reported catalysts in the literature and our Pd/NaY catalyst were

presented in Table S1. The activity and stability of the Pd/NaY catalyst for at least 150 h without deactivation was evaluated.

2.2. Catalytic reaction tests

The apparatus used for the reactivity tests was described elsewhere [17,33,34]. Reactions were carried out at atmospheric pressure in a fixed-bed quartz tube reactor (12 mm o.d. and 8 mm i.d.). The catalyst of 60–80 mesh was loaded into the uniform-temperature zone of the reactor, and the quartz wool was placed at both sides of the catalyst bed to fix the catalyst. The methyl nitrite (CH_3ONO) reactant was synthesized in laboratory through the esterification reaction ($2NaNO_2 + 2CH_3OH + H_2SO_4 \rightarrow 2CH_3ONO \uparrow + Na_2SO_4 + 2H_2O$). The generated CH_3ONO gas was collected into a stainless-steel cylinder and then mixed with pure N_2 to obtain a gas mixture of CH_3ONO: N_2 (1: 4, mole). The flow rates of N_2, CO: N_2 (1: 9; mole) and CH_3ONO: N_2 (1: 4; mole) gas mixtures were controlled by three calibrated mass flow meters. The reaction temperature and gas hourly space velocity (GHSV) were varied in the range of 30–125 ºC and 8000–1200000 mL g^{-1} h^{-1}, respectively. The stream leaving the reactor was analyzed by an online gas chromatography system (Agilent 7890B), equipped with a thermal conductivity detector (TCD) connected to 2.5 m molecular sieve 5A and 1.0 m HayeSep Q packed columns, and a flame ionization detector (FID) connected to 30 m HP-Innowax capillary column. The kinetic experiments, and the calculations of space time yield of DMC (STY_{DMC}), CH_3ONO

conversion, CO conversion, DMC, dimethoxymethane and methyl formate selectivity were presented in SI.

2.3. Catalyst characterization

Scanning electron microscopy (SEM) images were acquired on a JEOL JSM-7900F equipped with EDS. X-ray photoelectron spectroscopy (XPS) spectra were recorded on an Escalab 250xi spectrometer with an Al Kα radiation (binding energy was referenced to the C 1s peak at 284.6 eV).

In situ DRIFTS measurements were performed on a Bruker Vertex 70 spectrometer, equipped with a liquid-N_2-cooled highly sensitive mercury-cadmium-telluride (MCT) detector. The reaction chamber (Harrick Scientific HVC-DRP-4) included a diffuse reflectance cell with ZnSe windows, and a heating cartridge to obtain the desired temperature. Three calibrated mass flow meters were used to control the flow rates of N_2, CO: N_2 (1: 9; mole) and CH_3ONO: N_2 (1: 4; mole) gas mixtures. Prior to the DRIFTS experiments, the Pd/NaY catalyst was activated in the fixed-bed reactor by performing the reaction of DMC synthesis at 110 ºC for 3 h with a gas mixture of CO: CH_3ONO: N_2 (1: 6: 33; mole). In a typical process, 20 mg of used Pd/NaY catalyst after 3 h catalytic test was placed into the DRIFTS reaction cell, pre-treated with N_2 at 200 ºC for 1 h and cooled down to the desired temperature in N_2 for taking a background spectrum. In all cases, the flow rate of N_2 to the DRIFTS cell was 60 mL min^{-1} while other flow rates of gas mixtures were 15 mL

min^{-1}. The spectra were recorded in the range of 4000–600 cm^{-1} at a resolution of 4 cm^{-1} over 32 scans, if not specified. A series of carefully-designed *in situ* DRIFTS experiments were carried out as follows. First, for the adsorption of CO and CH_3ONO reactants, the pre-treated catalyst was exposed to the gas mixtures of CO: N_2 (1: 9; mole) or CH_3ONO: N_2 (1: 4; mole) at 30 ºC for 0.5 h, and flushed with N_2 at 30 ºC for 1 h. After that, the DRIFTS spectra were collected in the temperature range of 30–200 ºC. Second, for the steady-state reaction of DMC synthesis, the pre-treated catalyst was exposed to the gas mixture of CO: CH_3ONO: N_2 (1: 6: 33; mole) at 30 ºC for 0.5 h and then the DRIFTS spectrum was collected. Subsequently, the DRIFTS spectrum was recorded again at 30 ºC after N_2 purge for 1 h. Similarly, the spectra were collected at 50, 70, 90, 110 and 125 ºC as well. Third, for the dynamic pulse experiment of CO reactant, the pre-treated catalyst was exposed to the gas mixture of CH_3ONO: N_2 (1: 4; mole) at 30 ºC for 0.5 h; after N_2 purge for 1 h, a background spectrum was taken and subsequently, the gas mixture of CO: N_2 (1: 9; mole) was delivered into the DRIFTS cell with a pulse volume of 50 μL by N_2 carrier gas; the DRIFTS spectra were collected after each gas delivery at 30 ºC. Similarly, the spectra were recorded at 50, 70 and 90 ºC as well. For the dynamic pulse experiment using the CH_3ONO reactant, the pre-treated catalyst was exposed to the gas mixture of CO: N_2 (1: 9; mole) at 70 ºC for 0.5 h; after N_2 purge for 1 h, a background spectrum was taken and subsequently, the gas mixture of CH_3ONO: N_2 (1: 4; mole) was delivered into the cell, and the DRIFTS spectra were collected after each gas delivery at 70 ºC.

Similarly, the spectra were recorded at 90 ºC. Fourth, for the adsorption of methyl chloroformate (CH_3OCOCl), the pre-treated catalyst was kept at 30 ºC in N_2, then 2 μL CH_3OCOCl liquid was injected into the feed gas line, and introduced into the cell by N_2 carrier gas. After N_2 purge for 1 h, the spectra were collected in the temperature range of 30–200 ºC. Fifth, for the transient experiments, 3 μL HCl of 6 mol L^{-1} or pure CH_3OCOCl liquid was injected into the feed gas line, and introduced into the cell by the feed gas mixture of CO: CH_3ONO: N_2 (1: 6: 33; mole) at 110 ºC. The time-resolved DRIFTS spectra were collected at a rate of 8 spectra min^{-1} and accumulating 8 scans for each spectrum.

2.4. DFT calculations

A rhombohedral unit cell ($Si_{24}Al_{24}O_{96}$) of the faujasite structure with the $Fd\bar{3}$ space group symmetry was used to model the NaY zeolite catalyst. According to the Löwenstein rule, 12 Si atoms were substituted uniformly through the cell by 12 Al atoms to obtain a Si/Al molar ratio of 3.0 which is close to the Pd/NaY catalyst used in this work (Si/Al=2.8). Furthermore, 12 Na atoms were placed into the cell as follows: 2 Na atoms at site Ⅰ, 4 Na atoms at site I' and 6 Na atoms at site Ⅱ [35,36]. Since the Pd/NaY catalyst consisted of Pd^0 and Pd^{2+} species [17,23], a $Pd_{13}O_8$ cluster with mixed-valence Pd species, was embedded into the supercage of NaY ($Pd_{13}O_8$@NaY) to model the Pd/NaY catalyst.

Spin-polarized density functional theory (DFT) calculations were performed with

the generalized gradient approximation (GGA) [37] using the Perdew-Burke-Ernzerhof (PBE) [38] exchange-correlation potential. The dispersion correction (DFT-D3) based on the study of Grimme [39] was applied in the *Vienna Ab initio Simulation Package* (*VASP*) software [40]. The electron-ion interactions were described with the projector augmented wave (PAW) method [41]. An energy cutoff of 450 eV and Γ-centered *k*-points mesh of 1 × 1 × 1 were utilized for the calculations [42]. The climbing-image nudged elastic band (CI-NEB) method was combined with dimer method to find out the transition states (TS) between the reactants and products [43,44]. The energy on each atom was converged to 1×10^{-5} eV for the structure optimization. When the force threshold was less than 0.07 eV $Å^{-1}$, the convergence criterion was reached. In addition, the frequency calculations were conducted to check whether the stationary point was either a local minimum or a transition state (TS).

The energy barrier and the reaction energy were calculated as follows:

Energy barrier = $E_{TS} - E_R$

Reaction energy = $E_P - E_R$

where E_{TS}, E_R and E_P represent the total energies of the transition state, the reactant and the product in the elementary reaction, respectively.

3. Results and discussion

3.1. In situ DRIFTS study of dimethyl carbonate synthesis using Pd/NaY catalyst

3.1.1. DRIFTS study using CH_3ONO and CO reactants adsorbed on the Pd/NaY catalyst

The Pd/NaY catalyst was prepared by an ion-exchange method using $Pd(NH_3)_4^{2+}$ precursor. The low-temperature calcination at 200 ºC in air caused the $Pd(NH_3)_4^{2+}$ to lose partially the NH_3 ligands and to generate the $Pd(NH_3)_n^{2+}$ ($n < 2$) sites on the fresh catalyst [17]. The CO conversion and DMC selectivity changed drastically during the first hour of the catalytic test on the Pd/NaY catalyst in the indirect oxidative carbonylation of methanol to DMC; both the CO conversion and DMC selectivity did not change with extending the reaction time from 1 h to 6 h (Fig. S2). This suggested that the catalytic active sites for the DMC formation were gradually formed during the first hour of the catalytic test, possibly due to the disappearance of the remaining NH_3 ligands. This result was consistent with the TEM observation. Neither Pd clusters (below 2 nm) nor nanoparticles were observed on the fresh Pd/NaY catalyst before the catalytic test [23]. While Pd clusters with an average size of 1.3 nm on the used Pd/NaY catalyst were measured by HADDF-STEM [23]. Therefore, prior to the DRIFTS experiments, the Pd/NaY catalysts were activated in the fixed-bed reactor by performing the reaction of DMC synthesis at 110 ºC for 3 h with a gas mixture of CO: CH_3ONO: N_2 (1: 6: 33; mole).

Methyl nitrite, CH_3ONO is a reactive molecule due to the weak CH_3O–NO bond

(176 kJ mol^{-1}) [45,46]. The CH_3O–NO bond would be further weakened upon adsorption on the active metal surfaces [46]. The DRIFTS spectra of CH_3ONO adsorbed on the Pd/NaY catalyst are presented in Fig. 1. The bands at 2953, 2848 and 1080 cm^{-1} were assigned to CH_3 asymmetric, CH_3 symmetric and C–O stretching vibration (ν) respectively, corresponding to the OCH_3* (*, a surface site) species from the dissociative adsorption of CH_3ONO [47,48]. These OCH_3* species were stable below 150 ºC, but decomposed mostly at 200 ºC. The negative bands at 2953 cm^{-1} ($\nu_{as}(CH_3)$), 2848 cm^{-1} ($\nu_s(CH_3)$), and 1748 cm^{-1} (ν(C=O)) possibly characterized the residual reaction species such as $(CH_3O)_2CO$ on the used Pd/NaY catalyst after 3 h catalytic test (Fig. 1a–c). These negative bands were formed due to the desorption of residual reaction species [29]. The band at 1725 cm^{-1} ascribed to the linearly adsorbed NO* species was overlapped with the negative band at 1748 cm^{-1} [49]. The bands centered at 1576, 1509, 1446, 1393 and 1200 cm^{-1} were assigned to the nitrate and nitrite, formed by the reaction between the catalyst support and NO* species (Fig. 1a–d) [50,51]. To further confirm the effect of the desorption of residual reaction species, the used Pd/NaY catalyst after 3 h catalytic test was calcined in air at 200 ºC for 2 h, and then was employed for the adsorption of CH_3ONO. After eliminating the interference from the negative band at 1748 cm^{-1}, the band at 1725 cm^{-1} corresponding to the linearly adsorbed NO* species was clearly observed, [49] which was also presented in Fig. 1. After heating of the catalyst to 200 ºC together with the decomposition of the adsorbed CH_3ONO, the negative bands at 2953 cm^{-1} ($\nu_{as}(CH_3)$),

2848 cm^{-1} ($\nu_s(CH_3)$), and 1748 cm^{-1} ($\nu(C=O)$) appeared (Fig. S3). This suggested that the residual reaction species were on the surface of the used Pd/NaY catalyst. Moreover, the adsorption of CH_3ONO on the $Pd_{13}O_8$@NaY model was also conducted using DFT. However, the adsorption structure was unstable during the geometry optimization, and the dissociative adsorption of CH_3ONO occurred with a large adsorption energy of 492.9 kJ mol^{-1}. This suggested that the dissociation of CH_3ONO to CH_3O* and NO* was facile due to the weak CH_3O–NO bond. Combining the experimental and DFT approaches, it could be concluded that the dissociative adsorption of CH_3ONO readily occurred on the Pd/NaY catalyst, and provided the methoxy species (OCH_3*) for the DMC formation.

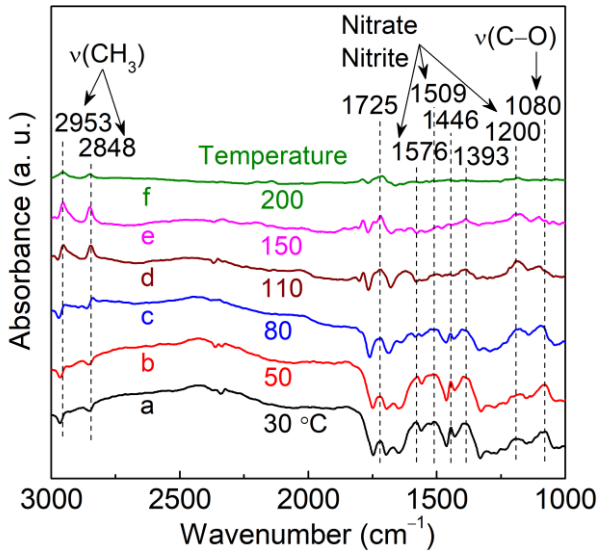

Fig. 1. DRIFTS spectra of CH_3ONO adsorbed on the Pd/NaY catalyst at different temperatures: (a) 30, (b) 50, (c) 80, (d) 110, (e) 150 and (f) 200 ºC. The Pd/NaY catalyst was pre-treated in N_2 at 200 ºC, cooled down to 30 ºC, and exposed to excess of gas mixture of CH_3ONO: N_2 (1: 4; mole) and purged by N_2.

Carbon monoxide is not only a common probe molecule but also the reactant in the DMC synthesis. Adsorption of CO on the Pd/NaY catalyst at 30 ºC was studied and the desorption behavior at increased temperature (Fig. 2). The well-defined bands centered at 2140 cm^{-1} and 2103 cm^{-1} were typically attributed to the linear CO adsorbed on the Pd^{2+} and Pd^{0} species, respectively [52,53]. A weak band at 1990 cm^{-1} was ascribed to the bridged CO adsorbed on the Pd^{0} species [54]. This was consistent with the XPS result confirming that both Pd^{2+} and Pd^{0} species were present on the Pd/NaY catalyst after the catalytic test (Fig. S4) [23]. With increasing the temperature from 30 ºC to 75 ºC, the band at 2140 cm^{-1} was gradually decreased, which was possibly due to the reduction of the cationic Pd by CO and/or the desorption of adsorbed CO species [55]. The bands at 2140, 2103 and 1990 cm^{-1} were present in the spectra recorded up to 100 ºC (Fig. 2). The CO adsorption experiment indicated that CO reactant was easily adsorbed on the Pd/NaY catalyst.

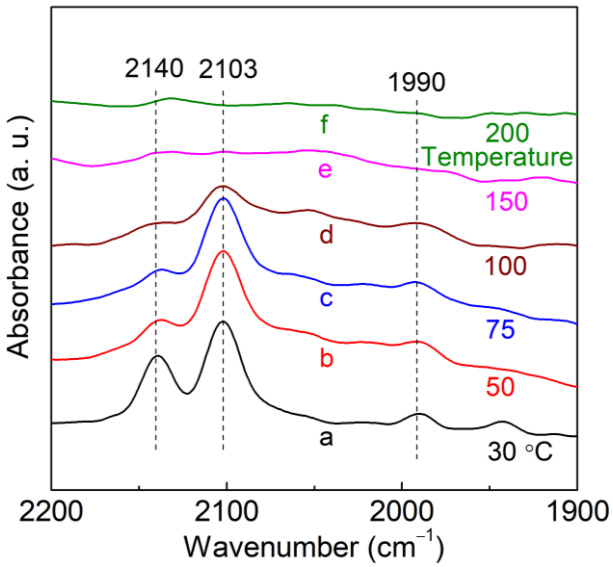

Fig. 2. DRIFTS spectra of CO adsorbed on the Pd/NaY catalyst at different

temperatures: (a) 30, (b) 50, (c) 75, (d) 100, (e) 150 and (f) 200 ºC. The Pd/NaY catalyst was pre-treated in N_2 at 200 ºC, cooled down to 30 ºC, and exposed to excess of gas mixture of CO: N_2 (1: 9; mole) and purged by N_2.

3.1.2. Steady-state reaction for dimethyl carbonate synthesis

In situ DRIFTS spectra of the steady-state reaction between CO and CH_3ONO reactants on the Pd/NaY catalyst are presented in Fig. 3A. In the case of exposing the catalyst to the gas mixture of CO: CH_3ONO: N_2 (1: 6: 33; mole) at 30 ºC, the doublet bands of gaseous CO were clearly observed at 2172 cm^{-1} and 2118 cm^{-1} (Fig. 3A,a). Compared to the spectrum of CH_3ONO gas shown in Fig. S5, the multiple bands in the range of 1687–1611 cm^{-1} were assigned to the gaseous CH_3ONO. With increasing the temperature from 30 ºC to 70 ºC, a new band at 2153 cm^{-1} appeared at 50 ºC, which was considerably enlarged at 70 ºC associated with the disappearance of gaseous CO bands at 2172 cm^{-1} and 2118 cm^{-1} (Fig. 3A,a–c). This newly emerged band at 2153 cm^{-1} was different from the bands at 2140 cm^{-1} (Pd^{2+}–CO species) and at 2103 cm^{-1} (Pd^0–CO species) (Fig. 2). The new band at 2153 cm^{-1} probably resulted from the reaction between CO and CH_3ONO reactants. As shown in Fig. 3A,c, the gaseous DMC and NO products started to form at 70 ºC which was evidenced by the appearance of characteristic bands at 1780 cm^{-1} due to the ν(C=O) of DMC and at 1909, 1845 cm^{-1} owing to the gaseous NO ($CO + 2CH_3ONO \rightarrow (CH_3O)_2CO + 2NO$ (the spectrum of gaseous DMC was shown in Fig. S5) [56]. A weak band at 1294

cm^{-1} appearing at 90 ºC corresponded to the ν(C–O) of gaseous DMC product (Fig. 3A,d). Both the bands at 2153 cm^{-1} and DMC product were gradually increased with the temperature increase from 70 ºC to 110 ºC (Fig. 3A,c–e). Indeed, the temperature-dependent evolution of the DMC product monitored by DRIFTS was in accordance with the fixed-bed reaction results: the space time yield of DMC improved remarkably from 0 to 0.13 $g_{DMC}\ g_{cat.}^{-1}\ h^{-1}$ with raising the reaction temperature from 50 ºC to 70 ºC, and reached a maximum of 0.73 $g_{DMC}\ g_{cat.}^{-1}\ h^{-1}$ at 110 ºC with a feed gas mixture of CO: CH_3ONO: N_2 (1: 6: 33; mole) at a gas hourly space velocity of 8000 mL $g_{cat.}^{-1}\ h^{-1}$ (Fig. S6).

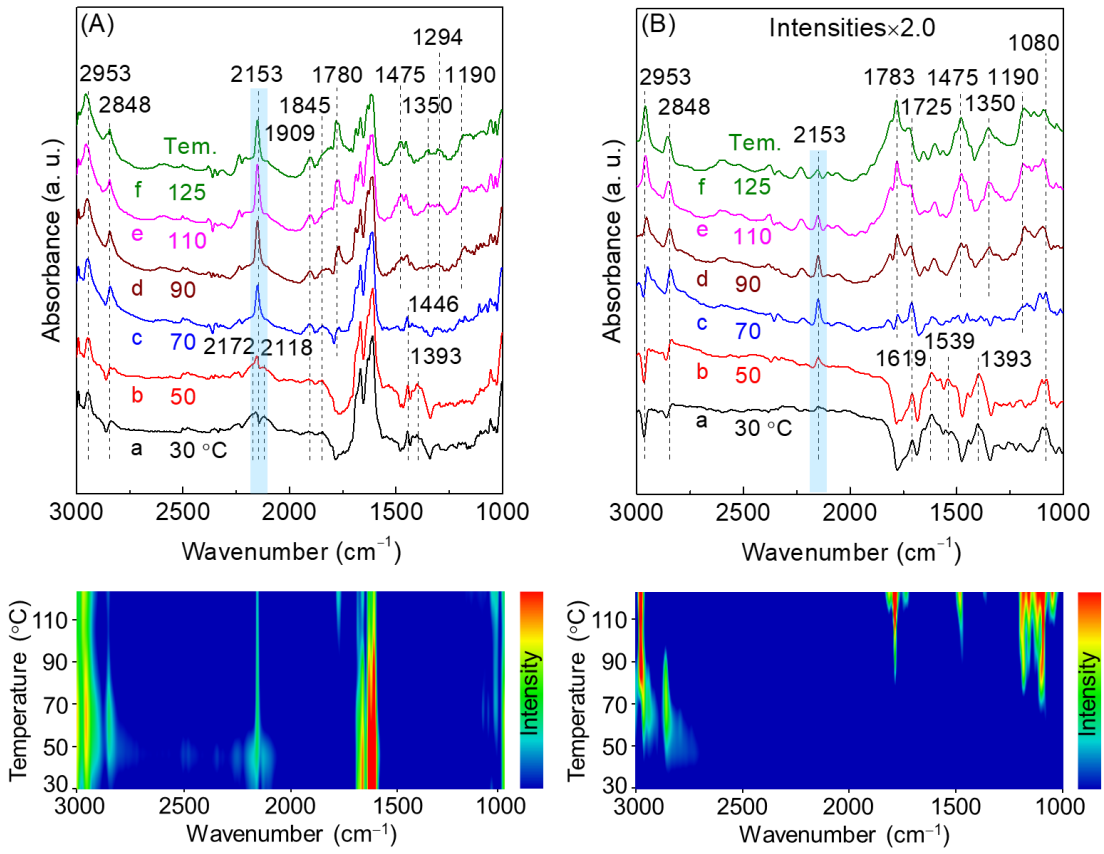

Fig. 3. DRIFTS spectra of (A) the steady-state reaction between CO and CH_3ONO reactants on the Pd/NaY catalyst and (B) the corresponding surface species after N_2

purge at different temperatures: (a) 30, (b) 50, (c) 70, (d) 90, (e) 110 and (f) 125 ºC. The sample was pre-treated in N_2 at 200 ºC, cooled down to 30 ºC, and exposed to the gas mixture of CO: CH_3ONO: N_2 (1: 6: 33; mole) for 0.5 h. The spectra in Fig. 3A,a and Fig. 3B,a were recorded at 30 ºC after N_2 purge for 1 h. The rest of the spectra were collected in the range of 50–125 ºC. Note that the intensities of all spectra in Fig. 3B were amplified by a factor of 2.0.

In order to detect the adsorbed surface species after the exposure of the Pd/NaY catalyst to CO and CH_3ONO reactants, the catalyst was thoroughly purged by N_2 and then the DRIFTS spectra were collected in the temperature range of 30–125 ºC (Fig. 3B). Clearly, the band at 2153 cm^{-1} was observed in all spectra. This suggested that the unknown species corresponding to the band at 2153 cm^{-1} were on the catalyst surface rather than in the gas phase. The intensity of the band at 2153 cm^{-1} increased gradually with raising the temperature from 30 ºC to 70 ºC due to the enhanced reaction rate, but declined with further increasing the temperature as the result of poor thermal stability of the species (Fig. 3B). The spectrum in Fig. 3B,c was different from the spectra in Fig. 3B,b,d (see the spectral range 1000–2000 cm^{-1}). The band at 1783 cm^{-1} of ν(C=O) appeared in the spectrum recorded at 70 ºC, which corresponded to the gaseous DMC product starting to be formed by exposing the catalyst to CO and CH_3ONO reactants (Fig. 3A,c and Fig. 3B,c). With increasing the temperature from 70 ºC to 125 ºC, the intensity of the bands at 1783, 1475, 1350 and

1190 cm^{-1} were remarkably increasing (Fig. 3B,c–f), which was consistent with the evolution of gaseous DMC product (Fig. 3A,c–f). In order to verify this result, the DMC was used as a probe molecule and adsorbed on the Pd/NaY catalyst. The DRIFTS spectrum collected from the DMC adsorbed on the catalyst contained the same bands at 1783, 1475, 1350 and 1190 cm^{-1} (Fig. S7). Thus, these bands were solidly assigned to the DMC product adsorbed on the catalyst (Fig. 3A,c–f and Fig. 3B,c–f). The multiple bands at 2953 cm^{-1} and 2848 cm^{-1} of $\nu(CH_3)$, and at 1080 cm^{-1} of ν(C–O) were also detected (Fig. 3B). In addition, the band at 1725 cm^{-1} was assigned to the linearly adsorbed NO* species, [49] which was consistent with the observation presented in Figs. 1 and 3B. The bands at 1619, 1539, 1446 and 1393 cm^{-1} due to the presence of nitrate and nitrite species were formed by the reaction between the zeolite support and the NO product (Fig. 3) [50,51].

3.1.3. Dynamic-pulse reaction after pre-adsorption of CH_3ONO and CO reactants

As stated above, the bands of reaction intermediates were likely overlapped with the strong bands of the CH_3ONO reactant and the DMC product in the steady-state DMC synthesis reaction (Fig. 3). To eliminate the interference of these strong bands, the background spectrum was taken after a pre-adsorption of the CH_3ONO reactant, and then the CO-pulse experiment was conducted to obtain the transient information; the results were shown in Fig. 4. In the case of performing the pulse reaction at 30 ºC, the first 5 pulses of CO reactant had a negligible effect on the DRIFTS spectra (Fig. 4A,a,b). After 10 pulses, two weak bands at 2963 cm^{-1} and 2851 cm^{-1} corresponding

to ν(CH_3), a band at 2153 cm^{-1} belonging to the unknown species, and a band at 1763 cm^{-1} related to ν(C=O) appeared (Fig. 4A,c). The intensities of these bands were remarkably enhanced after 40 pulses (Fig. 4A,g). It should be noted that the unknown species appearing at 2153 cm^{-1} were observed under both the CO pulse reaction and steady-state reaction (Figs. 3 and 4). The main question to be addressed here is the nature of the unknown species. As previously specified, the steady-state reaction indicated that the unknown species corresponding to the band at 2153 cm^{-1} resulted from the reaction between CO and CH_3ONO reactants (Fig. 3A). The species were related with the formation of DMC product (Fig. 3A), and existed on the catalyst surface rather than in the gas phase (Fig. 3B). As shown in Fig. 4A, the CH_3ONO reactant was pre-adsorbed on the Pd/NaY catalyst, and thus the Pd^0 active sites were oxidized to the Pd^{2+} through an oxidative-addition reaction (Pd^0 + CH_3ONO → $NO–Pd^{2+}–OCH_3$) [57]. The pulsed CO should lead to the formation of adsorbed CO species on the Pd^{2+} species. It was thus reasonable to infer that the pulsed CO could be adsorbed on the CH_3ONO-oxidized Pd^{2+} active sites, and thereby the unknown band at 2153 cm^{-1} was initially assigned to the formation of linearly adsorbed CO species on the CH_3ONO-oxidized Pd^{2+} active sites. This was in a good agreement with the reported results on linearly adsorbed CO species on Pd^{2+} species observed on the Pd catalysts under oxidation; the reported vibrational frequencies were in the range of 2150–2161 cm^{-1} [49,58–60].

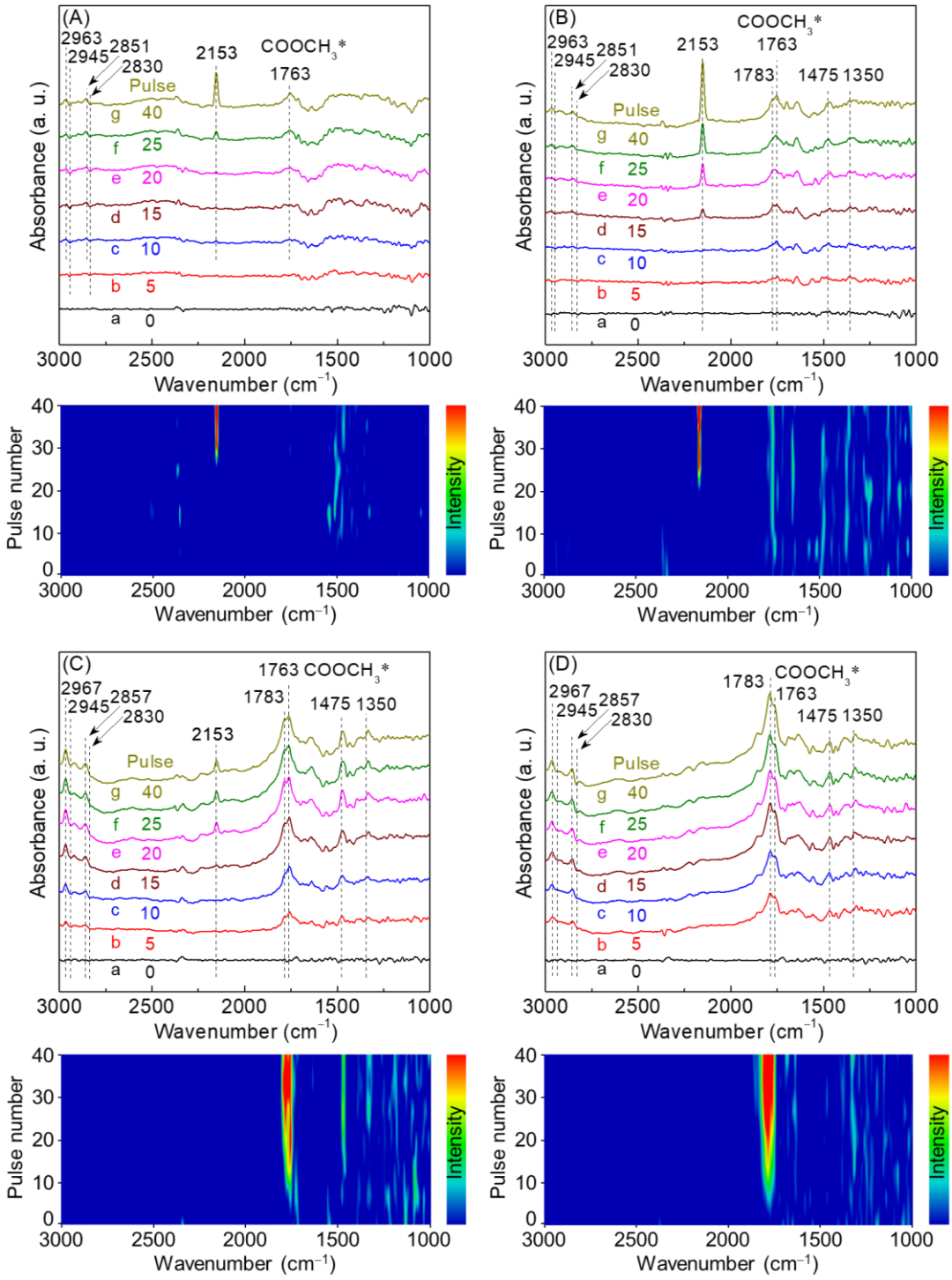

Fig. 4. Dynamic changes of DRIFTS spectra on the Pd/NaY catalyst with pre-adsorbed CH_3ONO reactant at (A) 30, (B) 50, (C) 70 and (D) 90 ºC as a function of CO pulses: (a) 0, (b) 5, (c) 10, (d) 15, (e) 20, (f) 25 and (g) 40. The sample was pre-treated in N_2 at 200 ºC, cooled down to 30 ºC, and exposed to the gas mixture of

CH_3ONO: N_2 (1: 4; mole) for 0.5 h; after N_2 purge for 1 h, a background spectrum was recorded and the spectra were recorded after the pulse of gas mixture of CO: N_2 reactant (1: 9; mole) at 30 ºC. Similarly, the spectra were collected at 50, 70 and 90 ºC too.

In the case of performing CO-pulse experiment at 50 ºC, the band at 1763 cm^{-1} corresponding to ν(C=O) emerged after the first 5 pulses (Fig. 4B,b). With increasing the CO pulse, the bands at 2153 cm^{-1} and 1763 cm^{-1} were gradually enhanced. Three weak bands at 1783, 1475 and 1350 cm^{-1} appeared, which were assigned to the DMC product adsorbed on the catalyst (Figs. 4B and S7). Since both the adsorbed CO species (2153 cm^{-1}) and the adsorbed DMC product (1783, 1475 and 1350 cm^{-1}) were detected, it was reasonable to infer that the adsorbed CO species could react with pre-adsorbed OCH_3* species to produce $COOCH_3$* intermediate, and $COOCH_3$* further coupled with OCH_3* forming DMC (CO* + OCH_3* → $COOCH_3$* + *; $COOCH_3$* + OCH_3* → $CO(OCH_3)_2$ + 2*). Thus, the unknown band at 1763 cm^{-1} in the carbonyl region was initially assigned to the $COOCH_3$* reaction intermediate. At 70 ºC and 90 ºC, the bands at 1783 cm^{-1} and 1763 cm^{-1} were clearly observed after the first 5 pulses (Fig. 4C,b and 4D,b). The band at 1763 cm^{-1} was more intense than that at 1783 cm^{-1} at 70 ºC (Fig. 4C,b), while the reverse result was obtained at 90 ºC (Fig. 4D,b). This indicated that more $COOCH_3$* intermediates were converted to DMC product due to the higher reaction rate at 90 ºC ($COOCH_3$* + OCH_3* →

$CO(OCH_3)_2$ + 2*). In addition, the bands at 2963 cm^{-1} and 2851 cm^{-1} of $\nu(CH_3)$ were detected at 30 and 50 ºC (Fig. 4A,4B). These two bands were shifted to 2967 cm^{-1} and 2857 cm^{-1} at 70 and 90 ºC, possibly because of the adsorbed DMC product (Fig. 4C,4D). Almost all the spectra for CO-pulse experiments performed at 30, 50, 70 and 90 ºC contained weak negative bands at 2945 cm^{-1} and 2830 cm^{-1}, which possibly were due to the desorption of pre-adsorbed OCH_3* species (Fig. 4).

To further confirm the chemical nature of the $COOCH_3$* intermediate, a probe molecule, methyl chloroformate (CH_3OCOCl) with the same $COOCH_3$ group was used. The molecular dynamics simulation of the CH_3OCOCl demonstrated that the bond length of C–Cl (0.18 nm) was larger than the counterparts of C–O (0.13 nm), C=O (0.12 nm) and C–H (0.11 nm). Therefore, the adsorption of the CH_3OCOCl probe molecule could reveal the $COOCH_3$* intermediate due to the cleavage of the C–Cl bond. Fig. 5 shows the DRIFTS spectra of the CH_3OCOCl adsorbed on the Pd/NaY catalyst at 30 ºC. The generated $COOCH_3$ species presented a characteristic band of ν(C=O) at 1775 cm^{-1}, which was similar to that of $COOCH_3$* intermediate at 1763 cm^{-1}. The bands at 2967, 1775 and 1441 cm^{-1} associated with the $COOCH_3$ species were detected in the temperature range of 30–125 ºC, suggesting that the $COOCH_3$ species were stable below 125 ºC (Fig. 5). We thus confirmed that the $COOCH_3$* intermediate could be captured at 30–90 ºC through the above CO-pulse experiments (Fig. 4).

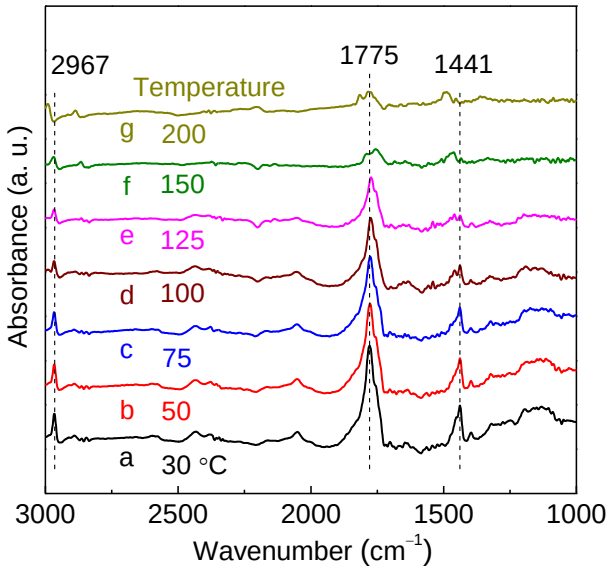

Fig. 5. DRIFTS spectra of methyl chloroformate (CH_3OCOCl) adsorbed on the Pd/NaY catalyst at different temperatures: (a) 30, (b) 50, (c) 75, (d) 100, (e) 125, (f) 150 and (g) 200 ºC. The sample was pre-treated in N_2 at 200 ºC, cooled down to 30 ºC, exposed to excess of CH_3OCOCl and purged by N_2. The spectra were recorded in the temperature range of 30–200 ºC; 2 μL CH_3OCOCl liquid was injected into the feed gas line and subsequently introduced into the DRIFTS cell.

Further the CH_3ONO-pulse experiment on the CO-pre-adsorbed Pd/NaY catalyst was conducted (Fig. 6). The band at 2153 cm^{-1} corresponding to the adsorbed CO species appeared after the first 5 pulses of CH_3ONO reactant at both temperatures (70 ºC and 90 ºC). This suggested that the pulsed CH_3ONO oxidized Pd^0 species to Pd^{2+} through an oxidative-addition reaction ($Pd^0 + CH_3ONO \rightarrow NO–Pd^{2+}–OCH_3$) [57], and thus the pre-adsorbed CO was converted into the new adsorbed CO species (2153 cm^{-1}) on the CH_3ONO-oxidized Pd^{2+} species. Along with the CH_3ONO pulse, the

band at 2153 cm^{-1} corresponding to the adsorbed CO species increased first and then decreased gradually due to the exhaustion of the pre-adsorbed CO on the catalyst (Fig. 6). The bands at 1783 cm^{-1} and 1763 cm^{-1} of ν(C=O) were not observed, that was possibly due to the overlapping with the negative bands formed by the CH_3ONO pulses (Fig. 6). As described above, the adsorption of CH_3ONO reactant would lead to multiple negative bands in the range of 1643–1775 cm^{-1} (Fig. 1). It should be noted that the newly formed species quickly appeared after the first 5 pulses of CH_3ONO reactant on the catalysts with pre-adsorbed CO at 70 ºC and 90 ºC (Fig. 6). While it took 25, 15, 5 and 5 pulses of CO reactant on the catalysts with pre-adsorbed CH_3ONO at 30, 50, 70 and 90 ºC, respectively (Fig. 4). One possible reason was that the surface Pd sites were reduced by the CO reactant. Such a reduction was more facile at higher temperatures and thus less pulses were needed before the newly formed species appeared. The formation rate of the species should be higher at elevated temperatures. In addition, the spectra of CH_3ONO-pulse experiments at 70 ºC and 90 ºC showed weak negative band at 1990 cm^{-1}, which was due to the desorption of pre-adsorbed CO* species (Fig. 6).

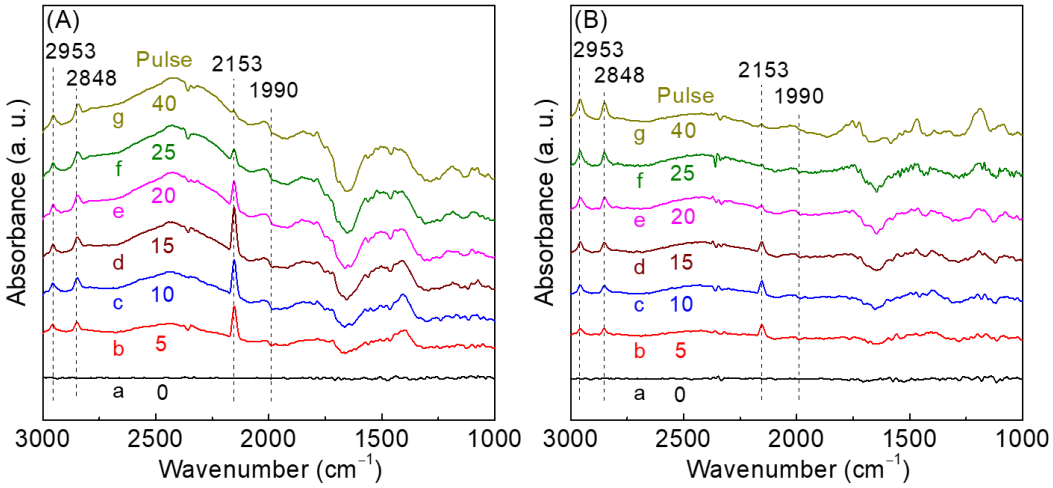

Fig. 6. Dynamic changes of DRIFTS spectra of the Pd/NaY catalyst with pre-adsorbed CO reactant at (A) 70 ºC and (B) 90 ºC as a function of CH_3ONO pulses: (a) 0, (b) 5, (c) 10, (d) 15, (e) 20, (f) 25 and (g) 40. The Pd/NaY catalyst was pre-treated in N_2 at 200 ºC, cooled down to 70 ºC, and exposed to the gas mixture of CO: N_2 (1: 9; mole) for 0.5 h. After N_2 purge for 1 h, a background spectrum was taken and finally, the spectra were recorded after the pulse of CH_3ONO: N_2 reactant (1: 4; mole) at 70 ºC. The spectra were collected at 90 ºC as well.

3.2. Catalytic reaction mechanism of dimethyl carbonate synthesis

Based on the above results, the main findings are summarized as follows. The adsorption experiments indicated that both CO and CH_3ONO reactants could be easily adsorbed on the Pd/NaY catalyst (Figs. 1 and 2). This was consistent with the DFT results showing the high adsorption energy of 198.8 kJ mol^{-1} for CO and 492.9 kJ mol^{-1} for CH_3O* and NO* species from the CH_3ONO dissociation on the $Pd_{13}O_8$@NaY catalyst model. The steady-state DMC synthesis reaction demonstrated

that the adsorbed CO species corresponding to the band at 2153 cm^{-1} was largely formed in the range of 70–125 ºC (Fig. 3). More importantly, the dynamic pulse reactions of CO on the CH_3ONO-pre-adsorbed catalyst indicated that the pre-adsorbed CH_3ONO could react with the adsorbed CO species to produce DMC (Fig. 4). Analogously, the dynamic-pulse reactions of CH_3ONO on the CO-pre-adsorbed catalyst suggested that the pre-adsorbed CO participated in the DMC formation (Fig. 6). All the information allowed us to affirm that the DMC synthesis followed the L-H mechanism, i.e., the adsorbed CO reacted with the adsorbed CH_3ONO.

The catalytic reaction mechanism describing the indirect oxidative carbonylation of methanol to DMC was proposed. The dissociative adsorption of CH_3ONO on Pd active sites was considered as the first step of the reaction thus providing the methoxy species (OCH_3*) for the DMC formation (Eq. 1; Fig. 1). The formation of the key reaction intermediate CO* on the CH_3ONO-oxidized Pd active sites was firmly confirmed through the steady-state and dynamic DRIFTS experiments (Eq. 2; Figs. 3 and 4). In particular, the abundant CO* intermediates were detected in the steady-state DMC synthesis at 110 ºC (Fig. 3), which was the optimal reaction temperature for the fixed-bed catalyst evaluation (Fig. S6). This suggested that the formation rate of the CO* intermediate was fast (Eq. 2), while the consumption rate of CO* was slow (Eq. 3) at the optimal temperature of 110 ºC. It could be thus inferred that the consumption of CO* (Eq. 3) was likely the rate-determining step in terms of the kinetics of

consecutive pathway for DMC synthesis [61,62]. Combining the dynamic pulse reactions and adsorption of CH_3OCOCl probe molecule, the $COOCH_3$* intermediate was identified (Figs. 4 and 5). The $COOCH_3$* could react with OCH_3* to form the $COOCH_3$* intermediate and further generated the DMC product (Eq. 4). The adsorbed NO* species desorbed directly or partially diffused from Pd active sites to the zeolite support to form nitrate and nitrite (Eq. 5).

$$2* + CH_3ONO \leftrightarrow NO* + OCH_3* \quad (1)$$

$$* + CO \leftrightarrow CO* \quad (2)$$

$$CO* + OCH_3* \rightarrow COOCH_3* + * \quad (3)$$

$$COOCH_3* + OCH_3* \leftrightarrow CO(OCH_3)_2 + 2* \quad (4)$$

$$NO* \leftrightarrow * + NO \quad (5)$$

The kinetic study of the catalytic reaction was often used to reveal the mechanism and reaction pathway [63,64]. A power-law kinetic equation was employed to describe the reaction rate of CO reactant: $-r_{CO} = k\, C_{CH_3ONO}^{\ a}\, C_{CO}^{\ b}$. As shown in Fig. 7, a regression analysis gave the reaction orders of 0.53 and –0.86 for CH_3ONO and CO, respectively. The reaction order of 0.53 for the CH_3ONO indicated that the reaction rate was positively associated with the CH_3ONO reactant [65], which was possibly due to its direct effect on the rate-determining step (Eq. 4). The reaction order of –0.86 for the CO was an indication of the inhibition effect. This was consistent with that the abundant CO* intermediates were detected in the steady-state DMC synthesis

reactions at 110 ºC (Fig. 3). The excessive CO* intermediates possibly occupied the active sites and inhibited the adsorption of CH_3ONO, and thereby decreased the formation rate of DMC [66]. Based on the Arrhenius equation, the apparent activation energy was estimated to be 66.8 kJ mol^{-1} (Fig. S8), which was similar to the reported values of 60–73 kJ mol^{-1} [17,18]. Therefore, the power-law kinetic equation on the Pd/NaY catalyst was established as $-r_{CO} = 2.86\times10^{9}\times exp(-66800/RT) \times C_{CH_3ONO}^{0.53} \times C_{CO}^{-0.86}$ ($mol_{CO}\ m_{cat.}^{-3}\ s^{-1}$), thus demonstrating a competitive L-H mechanism [67].

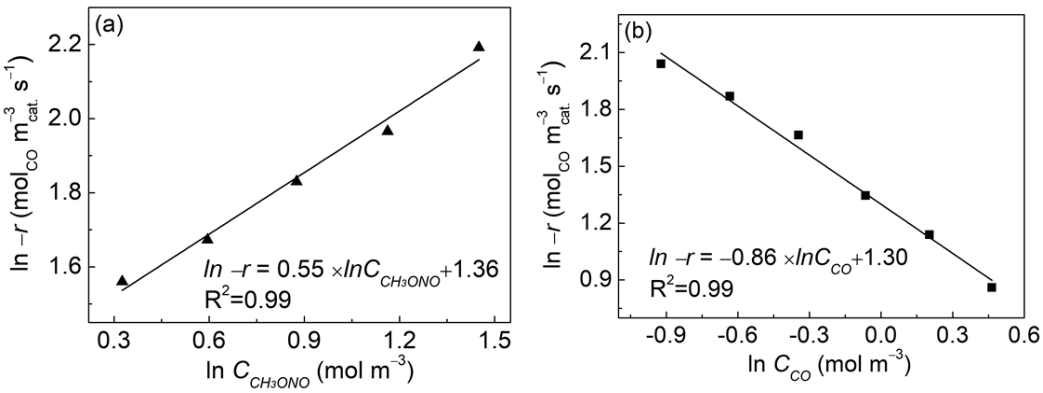

Fig. 7. The reaction orders of (a) CH_3ONO and (b) CO reactants for the indirect oxidative carbonylation of methanol to DMC over the Pd/NaY catalyst at 110 ºC. Reaction conditions: 0.1000 g mixture of catalyst and α-Al_2O_3 (diluent), CO: CH_3ONO: N_2 (1: 6: 33; mole), GHSV = 1200000 mL $g_{cat.}^{-1}\ h^{-1}$, 0.1 MPa. The feed gas mixtures of 3394–13578 Pa CH_3ONO, 1697 Pa CO, a balance of N_2 were used for the reaction order of CH_3ONO reactant, while 10136 Pa CH_3ONO, 1267–5066 Pa CO, a balance of N_2 were for CO reactant. The kinetic data were acquired within the differential regime and CO conversion was controlled below 10%. 0.0400 g catalyst

was mixed with 1.9600 g α-Al_2O_3, and then only 0.1000 g of the mixture was loaded for kinetic experiments.

The transient experiments using the CH_3OCOCl probe molecule were performed to validate the rate-determining step of DMC synthesis on the Pd/NaY catalyst. The rate-determining step was likely the generation of $COOCH_3$* intermediate (Eq. 4), and thus the formation rate of DMC (Eq. 5) should be proportional to the concentration of $COOCH_3$* on the catalyst surface. As previously stated, the dissociative adsorption of CH_3OCOCl on the Pd/NaY catalyst could form the $COOCH_3$* intermediate (Fig. 5). Therefore, the probe molecule CH_3OCOCl, i.e. $COOCH_3$* intermediate would react with the OCH_3* to generate DMC selectively, and thus improved the formation rate of DMC. When the reaction of DMC synthesis reached steady-state with a feed gas mixture of CO: CH_3ONO: N_2 (1: 6: 33; mole) at 110 ^oC, 3 μL CH_3OCOCl liquid was injected into the feed gas line and introduced into the DRIFTS reaction cell. Simultaneously, the time-resolved DRIFTS spectra were collected (Fig. S9). The band area of DMC product as a function of reaction time was evaluated from the spectra presented in Fig. S9, and shown in Fig. 8a. As expected, the band area of DMC increased remarkably along with the introduction of the CH_3OCOCl, and reached a maximum at 2.13 min (Fig. 8a). With prolonging the reaction time, the band area of DMC gradually decreased due to the exhaustion of the introduced CH_3OCOCl. For comparison, the CH_3OCOCl probe molecule of 3 μL was

introduced with the pure N_2 feed gas, and the band area of the CH_3OCOCl reached a maximum at 0.63 min (Fig. 8b). The experimental result was well fitted with a Gaussian distribution (Fig. 8b) [68]. The two curves in Fig. 8 showed different behavior, and this suggested that the introduction of CH_3OCOCl promoted the formation of DMC. To exclude the effect of chlorine, 3 μL HCl of 6 mol L^{-1} was injected into the feed gas line; a negligible impact of chlorine on the DMC formation was observed (Fig. S10). To quantify the addition of CH_3OCOCl, 3 μL CH_3OCOCl liquid with the feed gas mixture of CO: CH_3ONO: N_2 (1: 6: 33; mole) was introduced into a fixed-bed reactor, and the transient changes of space time yield of DMC (STY_{DMC}) were monitored by an online GC. As expected, STY_{DMC} was remarkably increased to 2.4–2.7 times using GHSV of 8000, 24000 and 48000 mL $g_{cat.}^{-1}$ h^{-1} (Table S2). These transient experiments further confirmed that the rate-determining step for DMC synthesis was the generation of the $COOCH_3$* intermediate (Eq. 4).

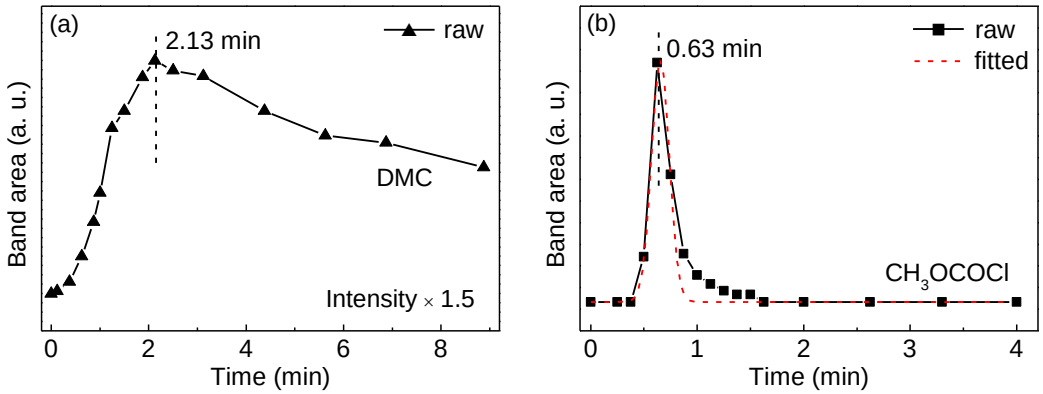

Fig. 8. (a) The area of the band at 1780 cm^{-1} corresponding to DMC from the DRIFTS spectra presented in Fig. S9A. 3 μL CH_3OCOCl liquid was injected into the feed gas line and then introduced into the DRIFTS reaction cell with the Pd/NaY

catalyst at 110 ºC. Simultaneously, the time-resolved DRIFTS spectra were collected. The feed gas mixture of CO: CH_3ONO: N_2 (1: 6: 33; mole) was used at a total flow rate of 15 mL min^{-1}. Note: the data presented in Fig. 8a were amplified by a factor of 1.5. (b) The area of the band at 1795 cm^{-1} corresponding to CH_3OCOCl from the DRIFTS spectra presented in Fig. S9B with the Gaussian fit. 3 μL CH_3OCOCl liquid was introduced into the DRIFTS reaction cell without catalyst using a feed gas of pure N_2 at 60 mL min^{-1}.

3.3. DFT calculations

DFT calculations were conducted to examine the reaction pathway of DMC synthesis from CO and CH_3ONO reactants. As shown in Fig. 9, a rhombohedral cell ($Na_{12}Si_{36}Al_{12}O_{96}$) of the faujasite structure was built to represent the NaY zeolite. A $Pd_{13}O_8$ cluster was embedded into the supercage of NaY ($Pd_{13}O_8$@NaY) to model the synthesized Pd/NaY catalyst [18,23]. The relative energy diagram for DMC formation, as well as the corresponding reactants, transition states (TS) and products structures were shown in Fig. 10. As previously stated, the CH_3ONO reactant was easily dissociated into OCH_3* and NO* species with a large adsorption energy of 492.9 kJ mol^{-1}; the adsorbed NO* species desorbed directly or partially diffused from Pd active sites to the zeolite support to form nitrate and nitrite (Figs. 1 and 3); the CO reactant was readily adsorbed forming CO* species (Fig. 2). As shown in Fig. 10, the co-adsorption of CO* and OCH_3* was easily generated. The OCH_3* through its

oxygen, approached the carbon of nearby CO* to form $COOCH_3$* intermediate via a transition state (TS-1), and this step needed to overcome a high energy barrier of 127.5 kJ mol^{-1}, accompanied by an endothermic heat of 3.8 kJ mol^{-1}. Subsequently, another OCH_3* species moved towards the carbon of $COOCH_3$* to generate the DMC via a transition state (TS-2) with an energy barrier of 58.8 kJ mol^{-1}, and it was exothermic by 22.2 kJ mol^{-1}. The results suggested that the step from OCH_3* and CO* to $COOCH_3$* was the rate-determining step with a high energy barrier of 127.5 kJ mol^{-1}. The DFT results further confirmed that the $COOCH_3$* was the key intermediate species, and the formation of $COOCH_3$* was the rate-determining step for the DMC synthesis. Table 1 summarizes the DFT-calculated and DRIFTS-experimentally observed frequencies of reaction intermediates for the DMC synthesis. The main experimental bands corresponding to OCH_3*, NO*, CO* and $COOCH_3$* species were consistent with the DFT calculations (Table 1). The DFT calculations further supported the assignments of the experimental bands.

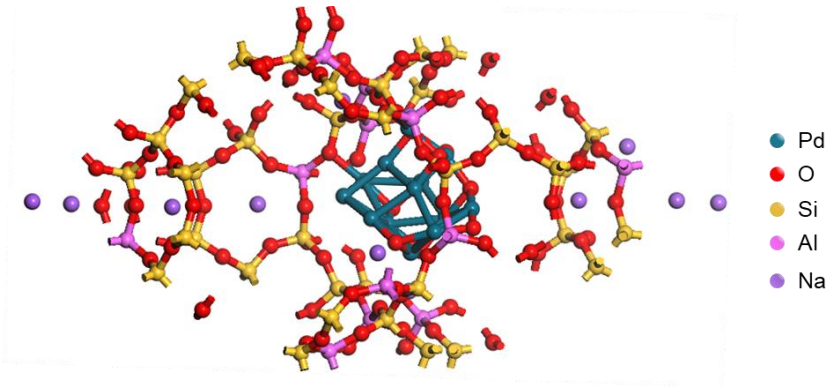

Fig. 9. The optimized structures of $Pd_{13}O_8$ cluster embedded in the supercage of the rhombohedral cell ($Na_{12}Si_{36}Al_{12}O_{96}$) of NaY zeolite ($Pd_{13}O_8$@NaY).

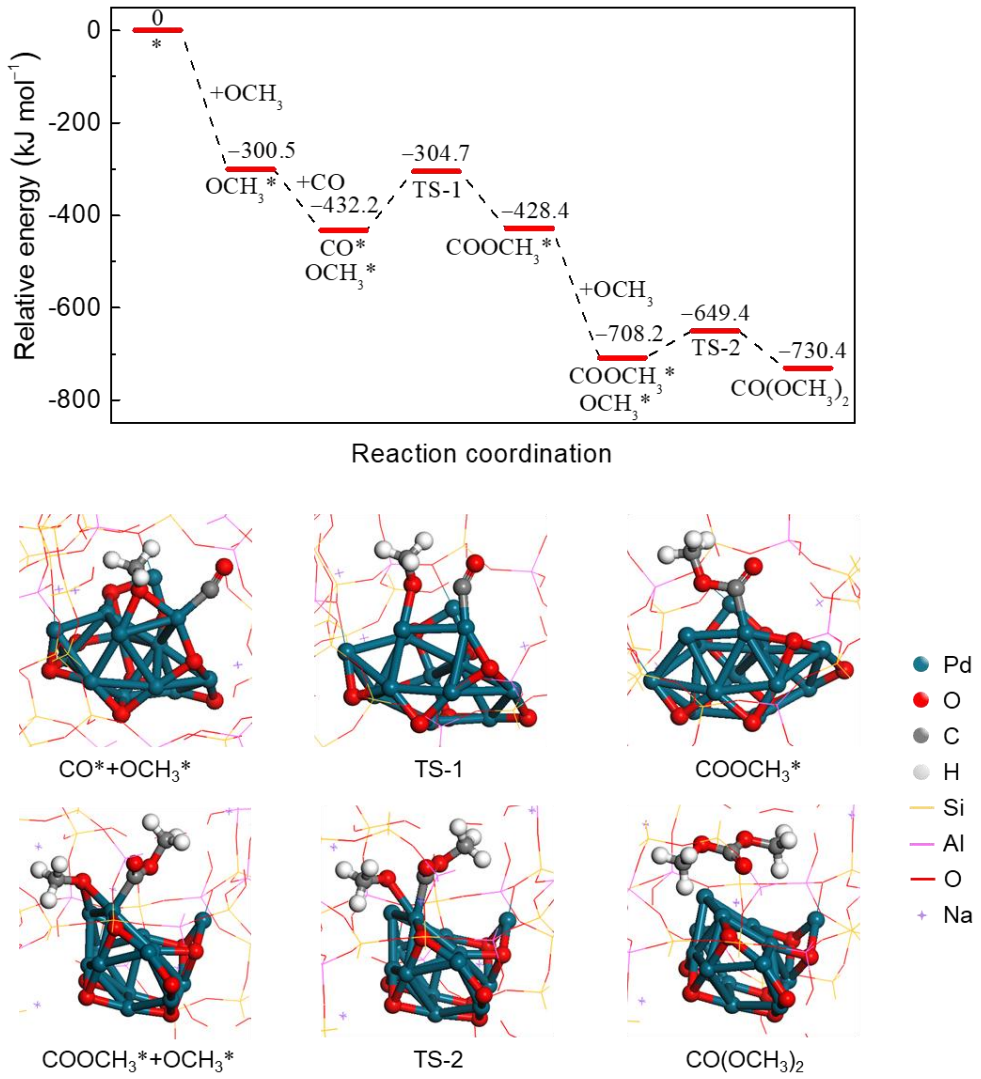

Fig. 10. Potential energy diagram for the DMC synthesis from CO and CH_3ONO together with the related reactant, transition state (TS) and product on the $Pd_{13}O_8$@NaY model. Blue, red, grey and white spheres represent Pd, O, C and H atoms, respectively. Yellow, pink and red sticks represent Si, Al and O atoms, and purple cross (✦) represent Na atoms.

Table 1 Vibrational frequencies of reaction intermediates for the DMC synthesis determined by DRIFTS and DFT calculations.

Intermediate	Bond	$\nu_{exp.}$ (cm^{-1})[a]	$\nu_{cal.}$ (cm^{-1})[b]
OCH_3*	C–O	1080	1084
NO*	N=O	1725	1766
CO*	C≡O	2153	2137[c]
$COOCH_3$*	C=O	1763	1754

[a] Frequencies determined by DRIFTS experiments.

[b] Frequencies from the DFT calculations. To facilitate comparison with experimental vibrational frequencies, a scaling factor of 1.05 was chosen due to the overestimation of interatomic distances in gradient-corrected DFT calculations [69,70].

[c] The adsorbed CO species on the $Pd_{13}O_8$@NaY model with pre-adsorbed CH_3ONO.

4. Conclusions

A series of *in situ* DRIFTS experiments combined with DFT calculations were performed to elucidate the catalytic reaction mechanism of the indirect oxidative carbonylation of methanol to DMC on the Pd/NaY catalyst. Two key reaction intermediates were captured evidently by steady-state, dynamic-pulse and time-resolved transient DRIFTS experiments, which were assigned to CO* and $COOCH_3$*. Based on the identification of the key intermediates, the reaction mechanism of the DMC synthesis was proposed including the following steps: (1) methyl nitrite (CH_3ONO) reactant dissociates into NO* and OCH_3*, (2) adsorbed

CO* reacts with OCH_3* to form $COOCH_3$*, and (3) another OCH_3* inserts into $COOCH_3$* to generate DMC. Abundant amount of CO* intermediates were detected on the catalyst surface in the steady-state reactions. DFT calculations also showed that the consumption of the CO* intermediate had higher energy barrier than other steps. This confirmed that the rate-determining step of DMC synthesis is the consumption of CO*, i.e., the insertion of OCH_3* into CO* to form $COOCH_3$*. The kinetic study resulted in a power-law equation of $-r_{CO} = 2.86\times10^{9}\times exp(-66800/RT) \times C_{CH_3ONO}^{0.53} \times C_{CO}^{-0.86}$ (mol_{CO} $m_{cat.}^{-3}$ s^{-1}). Our experimental and theoretical results provide important information for fine-tuning and design of high-performance catalysts for the indirect oxidative carbonylation of methanol to DMC.

Declaration of Competing Interest

The authors declare that they have no known competing financial interests or personal relationships that could have appeared to influence the work reported in this paper.

Acknowledgements

This work was supported by the National Natural Science Foundation of China (21908246, 21975285, 22175200, 21991090, 21991091) and the Sino-French International Associated Laboratory (LIA) “Zeolites”. Prof. Xinping Wu and Dr. Tingting Liu at the East China University of Science and Technology are acknowledged for their help with the DFT calculations.

References

[1] Z. Jin, L. Wang, E. Zuidema, K. Mondal, M. Zhang, J. Zhang, C. Wang, X. Meng, H. Yang, C. Mesters, F. Xiao, Hydrophobic Zeolite Modification for in Situ Peroxide Formation in Methane Oxidation to Methanol, Science 367 (2020) 193–197.

[2] W. Zhou, K. Cheng, J. Kang, C. Zhou, V. Subramanian, Q. Zhang, Y. Wang, New Horizon in C1 Chemistry: Breaking the Selectivity Limitation in Transformation of Syngas and Hydrogenation of CO_2 into Hydrocarbon Chemicals and Fuels, Chem. Soc. Rev. 48 (2019) 3193–3228.

[3] J. Bao, G. Yang, Y. Yoneyama, N. Tsubaki, Significant Advances in C1 Catalysis: Highly Efficient Catalysts and Catalytic Reactions, ACS Catal. 9 (2019) 3026–3053.

[4] P. Chen, G. Zhao, X. Shi, J. Zhu, J. Ding, Y. Lu, Nano-Intermetallic $InNi_3C_{0.5}$ Compound Discovered as a Superior Catalyst for CO_2 Reutilization, iScience 17 (2019) 315–324.

[5] P. Kumar, V.C. Srivastava, U.L. Štangar, B. Mušič, I.M. Mishra, Y. Meng, Recent Progress in Dimethyl Carbonate Synthesis Using Different Feedstock and Techniques in the Presence of Heterogeneous Catalysts, Catal. Rev. 63 (2021) 363–421.

[6] A.A. Pawar, D. Lee, W. Chung, H. Kim, Understanding the Synergy between MgO-CeO_2 as an Effective Promoter and Ionic Liquids for High Dimethyl

Carbonate Production from CO_2 and Methanol, Chem. Eng. J. 395 (2020) 124970.

[7] R. Saada, O. AboElazayem, S. Kellici, T. Heil, D. Morgan, G.I. Lampronti, B. Saha, Greener Synthesis of Dimethyl Carbonate Using a Novel Tin-Zirconia/Graphene Nanocomposite Catalyst, Appl. Catal. B 226 (2018) 451–462.

[8] Y. Chen, H. Wang, Z. Qin, S. Tian, Z. Ye, L. Ye, H. Abroshan, G. Li, $Ti_xCe_{1-x}O_2$ Nanocomposites: A Monolithic Catalyst for the Direct Conversion of Carbon Dioxide and Methanol to Dimethyl Carbonate, Green Chem. 21 (2019) 4642–4649.

[9] D. Dahnum, B. Seo, S. Cheong, U. Lee, J. Ha, H. Lee, Formation of Defect Site on ZIF-7 and Its Effect on the Methoxycarbonylation of Aniline with Dimethyl Carbonate, J. Catal. 380 (2019) 297–306.

[10] S. Huang, B. Yan, S. Wang, X. Ma, Recent Advances in Dialkyl Carbonates Synthesis and Applications, Chem. Soc. Rev. 44 (2015) 3079–3116.

[11] S. Uchiumi, K. Ataka, T. Matsuzaki, Oxidative Reactions by a Palladium-Alkyl Nitrite System, J. Organomet. Chem. 576 (1999) 279–289.

[12] N. Keller, G. Rebmann, V. Keller, Catalysts, Mechanisms and Industrial Processes for the Dimethylcarbonate Synthesis, J. Mol. Catal. A: Chem. 317 (2010) 1–18.

[13] Z. Wang, J. Sun, Z. Xu, G. Guo, CO Direct Esterification to Dimethyl Oxalate

and Dimethyl Carbonate: The Key Functional Motifs for Catalytic Selectivity, Nanoscale 12 (2020) 20131−20140.

[14] Y. Yamamoto, Phase Carbonylation Reactions Using Methyl Nitrite over Pd Catalysts, Catal. Surv. Asia 14 (2010) 103−110.

[15] H. Tan, Z. Wang, Z. Xu, J. Sun, Y. Xu, Q. Chen, Y. Chen, G. Guo, Review on the Synthesis of Dimethyl Carbonate, Catal. Today 316 (2018) 2−12.

[16] Y. Xu, Z. Wang, H. Tan, K. Jing, Z. Xu, G. Guo, Lewis Acid Sites in MOFs Supports Promoting the Catalytic Activity and Selectivity for CO Esterification to Dimethyl Carbonate, Catal. Sci. Technol. 10 (2020) 1699−1707.

[17] C. Wang, W. Xu, Z. Qin, H. Guo, X. Liu, S. Mintova, Highly Active Pd Containing EMT Zeolite Catalyst for Indirect Oxidative Carbonylation of Methanol to Dimethyl Carbonate, J. Energy Chem. 52 (2021) 191−201.

[18] Y. Dong, Y. Shen, Y. Zhao, S. Wang, X. Ma, Synergy between Palladium and Potassium Species for Efficient Activation of Carbon Monoxide in the Synthesis of Dimethyl Carbonate, ChemCatChem 7 (2015) 2460−2466.

[19] R. Guo, Y. Qin, L. Qiao, J. Chen, X. Wu, Y. Yao, Enhancement of the Catalytic Performance in Pd-Cu/NaY Catalyst for Carbonylation of Methyl Nitrite to Dimethyl Carbonate: Effects of Copper Doping, Catal. Commun. 88 (2017) 94–98.

[20] Y. Dong, S. Huang, S. Wang, Y. Zhao, J. Gong, X. Ma, Synthesis of Dimethyl Carbonate through Vapor-Phase Carbonylation Catalyzed by Pd-Doped Zeolites:

Interaction of Lewis Acidic Sites and Pd Species, ChemCatChem 5 (2013) 2174–2177.

[21] H. Tan, Z. Wang, Z. Xu, J. Sun, Z. Chen, Q. Chen, Y. Chen, G. Guo, Active Pd(Ⅱ) Complexes: Enhancing Catalytic Activity by Ligand Effect for Carbonylation of Methyl Nitrite to Dimethyl Carbonate, Catal. Sci. Technol. 7 (2017) 3785–3790.

[22] H. Tan, Z. Chen, Z. Xu, J. Sun, Z. Wang, R. Si, W. Zhuang, G. Guo, Synthesis of High-Performance and High-Stability Pd(II)/NaY Catalyst for CO Direct Selective Conversion to Dimethyl Carbonate by Rational Design, ACS Catal. 9 (2019) 3595–3603.

[23] C. Wang, N. Xu, T. Liu, W. Xu, H. Guo, Y. Li, P. Bai, X. Wu, X. Gong, X. Liu, S. Mintova, Mechanical Pressure-Mediated Pd Active Sites Formation in NaY Zeolite Catalysts for Indirect Oxidative Carbonylation of Methanol to Dimethyl Carbonate, J. Catal. 396 (2021) 269–280.

[24] Y. Yamamoto, T. Matsuzaki, S. Tanaka, K. Nishihira, K. Ohdan, A. Nakamura, Y. Okamoto, Catalysis and Characterization of Pd/NaY for Dimethyl Carbonate Synthesis from Methyl Nitrite and CO, J. Chem. Soc. Faraday Trans. 93 (1997) 3721–3727.

[25] L. Han, S. Cai, M. Gao, J. Hasegawa, P. Wang, J. Zhang, L. Shi, D. Zhang, Selective Catalytic Reduction of NO_x with NH_3 by Using Novel Catalysts: State of the Art and Future Prospects, Chem. Rev. 119 (2019) 10916–10976.

[26] L. Han, M. Gao, J. Hasegawa, S. Li, Y. Shen, H. Li, L. Shi, D. Zhang, SO_2-Tolerant Selective Catalytic Reduction of NO_x over Meso-TiO_2@Fe_2O_3@Al_2O_3 Metal-Based Monolith Catalysts, Environ. Sci. Technol. 53 (2019) 6462−6473.

[27] A.M. Abdel-Mageed, G. Kučerová, J. Bansmann, R.J. Behm, Active Au Species during the Low-Temperature Water Gas Shift Reaction on Au/CeO_2: A Time-Resolved Operando XAS and DRIFTS Study, ACS Catal. 7 (2017) 6471−6484.

[28] R. Mi, Z. Hu, B. Yang, In Situ DRIFTS for the Mechanistic Studies of 1,4-Butanediol Dehydration over Yb/Zr Catalysts, J. Catal. 370 (2019) 138−151.

[29] C. Wang, P. Chen, Y. Li, G. Zhao, Y. Liu, Y. Lu, In Situ DRIFTS Study of CO Coupling to Dimethyl Oxalate over Structured Al-Fiber@ns-AlOOH@Pd Catalyst, J. Catal. 344 (2016) 173−183.

[30] Z. Hu, X. Yong, D. Li, R.T. Yang, Synergism between Palladium and Nickel on Pd-Ni/TiO_2 for H_2-SCR: A Transient DRIFTS Study, J. Catal. 381 (2020) 204−214.

[31] K. Zha, C. Feng, L. Han, H. Li, T. Yan, S. Kuboon, L. Shi, D. Zhang, Promotional Effects of Fe on Manganese Oxide Octahedral Molecular Sieves for Alkali-Resistant Catalytic Reduction of NO_x: XAFS and in Situ DRIFTs Study, Chem. Eng. J. 381 (2020) 122764.

[32] F. Wang, S. He, H. Chen, B. Wang, L. Zheng, M. Wei, D.G. Evans, X. Duan,

Active Site Dependent Reaction Mechanism over Ru/CeO_2 Catalyst toward CO_2 Methanation, J. Am. Chem. Soc. 138 (2016) 6298−6305.

[33] C. Wang, W. Xu, Z. Qin, X. Liu, S. Mintova, Low-Temperature Synthesis of α-Alumina Nanosheets on Microfibrous-Structured Al-Fibers for Pd-Catalyzed CO Oxidative Coupling to Dimethyl Oxalate, Catal. Today 354 (2020) 158−166.

[34] C. Wang, W. Xu, Z. Qin, S. Mintova, Spontaneous Galvanic Deposition of Nanoporous Pd on Microfibrous-Structured Al-Fibers for CO Oxidative Coupling to Dimethyl Oxalate, Catal. Commun. 119 (2019) 39−41.

[35] T. Frising, P. Leflaive, Extraframework Cation Distributions in X and Y Faujasite Zeolites: A Review, Microporous Mesoporous Mater. 114 (2008) 27−63.

[36] A.A. Rybakov, A.V. Larin, D.P. Vercauteren, CO Diffusion as a Re-Orientation Mechanism in the NaY Zeolite, Phys. Chem. Chem. Phys. 19 (2017) 20930−20940.

[37] Perdew, Chevary, Vosko, Jackson, Pederson, Singh, Fiolhais, Atoms, Molecules, Solids, and Surfaces: Applications of the Generalized Gradient Approximation for Exchange and Correlation, Phys. Rev. B 46 (1992) 6671−6687.

[38] J.P. Perdew, K. Burke, M. Ernzerhof, Generalized Gradient Approximation Made Simple, Phys. Rev. Lett. 77 (1996) 3865−3868.

[39] S. Grimme, S. Ehrlich, L. Goerigk, Effect of the Damping Function in

Dispersion Corrected Density Functional Theory, J. Comput. Chem. 32 (2011) 1456–1465.

[40] J. Hafner, Ab-Initio Simulations of Materials Using VASP: Density-Functional Theory and Beyond, J. Comput. Chem. 29 (2008) 2044–2078.

[41] D. Joubert, G. Kresse, From Ultrasoft Pseudopotentials to the Projector Augmented-Wave Method, Phys. Rev. B 59 (1999) 1758–1775.

[42] A.M. Vos, X. Rozanska, R.A. Schoonheydt, R.A. van Santen, F. Hutschka, J. Hafner, Theoretical Study of the Alkylation Reaction of Toluene with Methanol Catalyzed by Acidic Mordenite, J. Am. Chem. Soc. 123 (2001) 2799–2809.

[43] D. Sheppard, P. Xiao, W. Chemelewski, D.D. Johnson, G. Henkelman, A Generalized Solid-State Nudged Elastic Band Method, J. Chem. Phys. 136 (2012) 074103.

[44] J. Kästner, P. Sherwood, Superlinearly Converging Dimer Method for Transition State Search, J. Chem. Phys. 128 (2008) 014106.

[45] C.J. Cassady, B.S. Freiser, Gas-Phase Reactions of Transition-Metal Ions with Methyl Nitrite and Nitromethane, J. Am. Chem. Soc. 107 (1985) 1566–1573.

[46] J.W. Peck, D.E. Beck, D.I. Mahon, B.K. Koel, Methyl Nitrite Adsorption as a Novel Route to the Surface Methoxy Intermediate, J. Phys. Chem. B 102 (1998) 3321–3323.

[47] Z. Sun, X. Zhang, H. Li, T. Liu, S. Sang, S. Chen, L. Duan, L. Zeng, W. Xiang, J. Gong, Chemical Looping Oxidative Steam Reforming of Methanol: A New

Pathway for Auto-Thermal Conversion, Appl. Catal. B 269 (2020) 118758.

[48] F. Zhao, G. Zhan, S. Zhou, Intercalation of Laminar Cu-Al LDHs with Molecular TCPP(M) (M = Zn, Co, Ni, and Fe) towards High-Performance CO_2 Hydrogenation Catalysts, Nanoscale 12 (2020) 13145–13156.

[49] N. Macleod, R. Cropley, J.M. Keel, R.M. Lambert, Exploiting the Synergy of Titania and Alumina in Lean NO_x Reduction: In Situ Ammonia Generation during the $Pd/TiO_2/Al_2O_3$-Catalysed $H_2/CO/NO/O_2$ Reaction, J. Catal. 221 (2004) 20–31.

[50] W.S. Kijlstra, D.S. Brands, E.K. Poels, A. Bliek, Mechanism of the Selective Catalytic Reduction of NO by NH_3 over MnO_x/Al_2O_3, J. Catal. 171 (1997) 208–218.

[51] F.C. Meunier, J.P. Breen, V. Zuzaniuk, M. Olsson, J.R.H. Ross, Mechanistic Aspects of the Selective Reduction of NO by Propene over Alumina and Silver-Alumina Catalysts, J. Catal. 187 (1999) 493–505.

[52] K. Khivantsev, N.R. Jaegers, L. Kovarik, J.C. Hanson, F.F. Tao, Y. Tang, X. Zhang, I.Z. Koleva, H.A. Aleksandrov, G.N. Vayssilov, Y. Wang, F. Gao, J. Szanyi, Achieving Atomic Dispersion of Highly Loaded Transition Metals in Small-Pore Zeolite SSZ-13: High-Capacity and High-Efficiency Low-Temperature CO and Passive NO_x Adsorbers, Angew. Chem. Int. Ed. 57 (2018) 16672–16677.

[53] Y. Ji, S. Bai, D. Xu, D. Qian, Z. Wu, Y. Song, R. Pace, M. Crocker, K. Wilson,

A. Lee, D. Harris, D. Scapens, Pd-Promoted WO_3-ZrO_2 for Low Temperature NO_x Storage, Appl. Catal. B 264 (2020) 118499.

[54] M. Ambast, K. Karinshak, B.M.M. Rahman, L.C. Grabow, M.P. Harold, Passive NO_x Adsorption on Pd/H-ZSM-5: Experiments and Modeling, Appl. Catal. B 269 (2020) 118802.

[55] C. Wang, L. Han, P. Chen, G. Zhao, Y. Liu, Y. Lu, High-Performance, Low Pd-Loading Microfibrous-Structured Al-Fiber@ns-AlOOH@Pd Catalyst for CO Coupling to Dimethyl Oxalate, J. Catal. 337 (2016) 145–156.

[56] C. Wang, Y. Jia, Z. Zhang, G. Zhao, Y. Liu, Y. Lu, Role of PdC_x Species in Pd@PdC_x/AlOOH/Al-Fiber Catalyst for the CO Oxidative Coupling to Dimethyl Oxalate, Appl. Surf. Sci. 478 (2019) 840–845.

[57] Z. Gao, Z. Liu, F. He, G. Xu, Combined XPS and in Situ DRIRS Study of Mechanism of Pd-Fe/alpha-Al_2O_3 Catalyzed CO Coupling Reaction to Diethyl Oxalate, J. Mol. Catal. A: Chem. 235 (2005) 143–149.

[58] T. Baidya, P. Bera, B.D. Mukri, S.K. Parida, O. Kröcher, M. Elsener, M.S. Hegde, DRIFTS Studies on CO and NO Adsorption and NO+CO Reaction over Pd^{2+}-Substituted CeO_2 and $Ce_{0.75}Sn_{0.25}O_2$ Catalysts, J. Catal. 303 (2013) 117–129.

[59] M. Valden, R.L. Keiski, N. Xiang, J. Pere, J. Aaltonen, M. Pessa, T. Maunula, A. Savimäki, A. Lahti, M. Härkönen, Reactivity of Pd/Al_2O_3, Pd/La_2O_3-Al_2O_3 and Pd/$LaAlO_3$ Catalysts for the Reduction of NO by CO: CO and NO

Adsorption, J. Catal. 161 (1996) 614–625.

[60] A. Martínez-Arias, M. Fernández-García, A. Iglesias-Juez, A.B. Hungría, J.A. Anderson, J.C. Conesa, J. Soria, New Pd/$Ce_xZr_{1-x}O_2$/Al_2O_3 Three-Way Catalysts Prepared by Microemulsion: Part 2. In Situ Analysis of CO Oxidation and NO Reduction under Stoichiometric CO+NO+O_2, Appl. Catal. B 31 (2001) 51–60.

[61] M.A. Vasiliades, C.M. Kalamaras, N.S. Govender, A. Govender, A.M. Efstathiou, The Effect of Preparation Route of Commercial Co/γ-Al_2O_3 Catalyst on Important Fischer-Tropsch Kinetic Parameters Studied by SSITKA and CO-DRIFTS Transient Hydrogenation Techniques, J. Catal. 379 (2019) 60–77.

[62] R. Pestman, W. Chen, E. Hensen, Insight into the Rate-Determining Step and Active Sites in the Fischer-Tropsch Reaction over Cobalt Catalysts, ACS Catal. 9 (2019) 4189–4195.

[63] A.D. Allian, K. Takanabe, K.L. Fujdala, X. Hao, T.J. Truex, J. Cai, C. Buda, M. Neurock, E. Iglesia, Chemisorption of CO and Mechanism of CO Oxidation on Supported Platinum Nanoclusters, J. Am. Chem. Soc. 133 (2011) 4498–4517.

[64] Z. Mao, C.T. Campbell, Apparent Activation Energies in Complex Reaction Mechanisms: A Simple Relationship via Degrees of Rate Control, ACS Catal. 9 (2019) 9465–9473.

[65] H. Guan, J. Lin, L. Li, X. Wang, T. Zhang, Highly Active Subnano Rh/$Fe(OH)_x$ Catalyst for Preferential Oxidation of CO in H_2-Rich Stream, Appl. Catal. B 184 (2016) 299–308.

[66] X. Liao, Y. Liu, W. Chu, S. Sall, C. Petit, V. Pitchon, V. Caps, Promoting Effect of AuCu Alloying on Au-Cu/CeO_2-Catalyzed CO Oxidation: A Combined Kinetic and in Situ DRIFTS Study, J. Catal. 382 (2020) 329–338.

[67] N. Li, Q. Chen, L. Luo, W. Huang, M. Luo, G. Hu, J. Lu, Kinetic Study and the Effect of Particle Size on Low Temperature CO Oxidation over Pt/TiO_2 Catalysts, Appl. Catal. B 142–143 (2013) 523–532.

[68] K. Abou Hweij, F. Azizi, Hydrodynamics and Residence Time Distribution of Liquid Flow in Tubular Reactors Equipped with Screen-Type Static Mixers, Chem. Eng. J. 279 (2015) 948–963.

[69] S. Jones, J. Qu, K. Tedsree, X. Gong, S.C.E. Tsang, Prominent Electronic and Geometric Modifications of Palladium Nanoparticles by Polymer Stabilizers for Hydrogen Production under Ambient Conditions, Angew. Chem. Int. Ed. 51 (2012) 11275–11278.

[70] I.V. Yudanov, R. Sahnoun, K.M. Neyman, N. Rösch, J. Hoffmann, S. Schauermann, V. Johánek, H. Unterhalt, G. Rupprechter, J. Libuda, H. Freund, CO Adsorption on Pd Nanoparticles: Density Functional and Vibrational Spectroscopy Studies, J. Phys. Chem. B 107 (2003) 255–264.